Corrections

MEDICAL SCIENCES

Correction for "Genetic confirmation for a central role for TNFα in the direct action of thyroid stimulating hormone on the skeleton," by Li Sun, Ling-Ling Zhu, Ping Lu, Tony Yuen, Jianhua Li, Risheng Ma, Ramkumari Baliram, Surinder S. Moonga, Peng Liu, Alberta Zallone, Maria I. New, Terry F. Davies, and Mone Zaidi, which appeared in issue 24, June 11, 2013, of *Proc Natl Acad Sci USA* (110:9891–9896; first published May 28, 2013; 10.1073/pnas.1308336110).

The authors note that the author name Ramkumari Baliram should instead appear as Ramkumarie Baliram. The corrected author line appears below. The online version has been corrected.

Li Sun, Ling-Ling Zhu, Ping Lu, Tony Yuen, Jianhua Li, Risheng Ma, Ramkumarie Baliram, Surinder S. Moonga, Peng Liu, Alberta Zallone, Maria I. New, Terry F. Davies, and Mone Zaidi

www.pnas.org/cgi/doi/10.1073/pnas.1311771110

MICROBIOLOGY

Correction for "IKK epsilon kinase is crucial for viral G protein-coupled receptor tumorigenesis," by Yi Wang, Xiaolu Lu, Lining Zhu, Yan Shen, Shylet Chengedza, Hao Feng, Laiyee Wang, Jae U. Jung, Julio S. Gutkind, and Pinghui Feng, which appeared in issue 27, July 2, 2013, of *Proc Natl Acad Sci USA* (110:11139–11144; first published June 14, 2013; 10.1073/pnas.1219829110).

The authors note that the author name Julio S. Gutkind should instead appear as J. Silvio Gutkind. The corrected author line appears below. The online version has been corrected.

Yi Wang, Xiaolu Lu, Lining Zhu, Yan Shen, Shylet Chengedza, Hao Feng, Laiyee Wang, Jae U. Jung, J. Silvio Gutkind, and Pinghui Feng

www.pnas.org/cgi/doi/10.1073/pnas.1312158110

ANTHROPOLOGY

Correction for "Beginning of viniculture in France," by Patrick E. McGovern, Benjamin P. Luley, Nuria Rovira, Armen Mirzoian, Michael P. Callahan, Karen E. Smith, Gretchen R. Hall, Theodore Davidson, and Joshua M. Henkin, which appeared in issue 25, June 18, 2013, of *Proc Natl Acad Sci USA* (110:10147–10152; first published June 3, 2013; 10.1073/pnas.1216126110).

The authors note that on page 10151, left column, fourth full paragraph, lines 8–11, "However, such exploitation and the morphological transition between wild and domestic grapes is not attested until at least the third century B.C., particularly at Port Ariane, about a half kilometer distant from Lattara (26)" should instead appear as "However, such exploitation and the morphological transition between wild and domestic grapes is not attested until at least the seventh–sixth century B.C., particularly at Port Ariane, about a half kilometer distant from Lattara (26)."

www.pnas.org/cgi/doi/10.1073/pnas.1312239110

PHYSICS

Correction for "Elasto-inertial turbulence," by Devranjan Samanta, Yves Dubief, Markus Holzner, Christof Schäfer, Alexander N. Morozov, Christian Wagner, and Björn Hof, which appeared in issue 26, June 25, 2013, of *Proc Natl Acad Sci USA* (110:10557–10562; first published June 11, 2013; 10.1073/pnas.1219666110).

The authors note that the following statement should be added to the Acknowledgments: "Y.D. gratefully acknowledges the Vermont Advanced Computing Core, supported by NASA (NNX-08AO96G), which provided the computational resources."

www.pnas.org/cgi/doi/10.1073/pnas.1311539110

Elasto-inertial turbulence

Devranjan Samanta[a,b], Yves Dubief[c], Markus Holzner[a], Christof Schäfer[b], Alexander N. Morozov[d], Christian Wagner[b], and Björn Hof[a,e,1]

[a]Max Planck Institute for Dynamics and Self-Organization, 37073 Göttingen, Germany; [b]Experimental Physics, Saarland University, 66041 Saarbrücken, Germany; [c]School of Engineering, University of Vermont, Burlington, VT 05405; [d]Scottish Universities Physics Alliance, School of Physics and Astronomy, University of Edinburgh, Edinburgh EH9 3JZ, United Kingdom; and [e]Institute of Science and Technology Austria, 3400 Klosterneuburg, Austria

Edited* by Katepalli R. Sreenivasan, New York University, New York, NY, and approved May 3, 2013 (received for review November 11, 2012)

Turbulence is ubiquitous in nature, yet even for the case of ordinary Newtonian fluids like water, our understanding of this phenomenon is limited. Many liquids of practical importance are more complicated (e.g., blood, polymer melts, paints), however; they exhibit elastic as well as viscous characteristics, and the relation between stress and strain is nonlinear. We demonstrate here for a model system of such complex fluids that at high shear rates, turbulence is not simply modified as previously believed but is suppressed and replaced by a different type of disordered motion, elasto-inertial turbulence. Elasto-inertial turbulence is found to occur at much lower Reynolds numbers than Newtonian turbulence, and the dynamical properties differ significantly. The friction scaling observed coincides with the so-called "maximum drag reduction" asymptote, which is exhibited by a wide range of viscoelastic fluids.

elastic instabilities | polymer drag reduction | non-Newtonian fluids | transition to turbulence

The most efficient method with which to reduce the large drag of turbulent flows of liquids is through addition of small amounts of polymers or surfactants. As first observed in the 1940s (1), frictional losses can be reduced by more than 70% (2, 3), and this technique has found application in oil pipelines, sewage, heating, and irrigation networks (4, 5). For dilute solutions, the drag is found to reduce with polymer concentration and eventually approaches an empirically found limit, the maximum drag reduction (MDR) asymptote (6, 7). A number of theories have been put forward to explain the mechanism of drag reduction and the origin of the MDR asymptote (3). Most of them invoke the elasticity of long polymer molecules: They are stretched in strong shear and elongational flow, and they recoil in vortical regions. It has been shown that this process inhibits vortices, and hence suppresses the turbulence-sustaining mechanism (8–15). It has recently been proposed that such inhibition may bring dynamics of drag-reducing flows close to the low-dimensional structures that separate turbulent and laminar flows in Newtonian turbulence (16), and it has been argued that the MDR asymptote is a consequence of the marginal dynamics on this separating boundary. Regarding the effect of polymers on the onset of turbulence, seemingly conflicting observations have been reported. Many investigations reported transition delay (ref. 17 and references therein); that is, the onset was postponed to a higher Reynolds number (*Re*; defined as a ratio of inertial to viscous forces). In other studies (18–20) (largely in pipes of small diameter), it has been observed that turbulence sets in at a *Re* smaller than in the Newtonian case, a phenomenon termed "early turbulence." However, in other studies (17, 21), investigators found that the natural transition point of their pipe experiment (i.e., the point where the flow becomes turbulent without additional perturbations) moved to a lower *Re* compared with the Newtonian case.

Although the addition of small amounts of polymer reduces the drag at a large *Re*, its effect is dramatically different at a very small *Re*. In this regime, the flow is controlled by polymer stretching, orientation, and relaxation, which give rise to anisotropic elastic stresses in the fluid. The magnitude of these stresses, and the degree of their anisotropy, is set by the product of the longest relaxation time of polymer molecules and a typical shear rate, the so-called Weissenberg number (*Wi*). It has recently been demonstrated that at a large *Wi*, the anisotropic elastic stresses destabilize flows with curved streamlines even in the absence of inertia, resulting in so-called "purely elastic linear instabilities" (22, 23). At a yet higher *Wi*, these instabilities are followed by a unique type of disordered motion called elastic turbulence, which exhibits fluctuations at many spatial and temporal scales (24, 25). A direct transition from laminar to turbulent flows has also been observed for flows in curved channels (25). In parallel shear geometries, like flow in straight pipes, purely linear elastic instabilities are absent (26); however, in principle, there can be a subcritical transition to elastic turbulence and strong evidence for such a transition has been found (27–29).

Presently, very little is known about possible interaction between the two phenomena, Newtonian and elastic turbulence. The existing theories of drag reduction all share the same conceptual feature: They interpret the resulting flow as a modified form of ordinary Newtonian shear flow turbulence, with its properties being determined by the balance between elastic and viscous stresses (11, 15, 16, 30, 31). Theoretical studies of the influence of polymers on turbulence in unbounded (30–32) flows, however, showed some qualitative differences from Newtonian turbulence; in one case (32), the measured power spectra more closely resembled those found in elastic turbulence than those in Newtonian flows.

Here, we perform experiments on viscoelastic pipe flow and observe that addition of small amounts of polymer postpones the transition to Newtonian turbulence. However, we find that, additionally, there exists a different type of chaotic motion, controlled by the elastic stresses, that can set in at a lower *Re* than in the Newtonian case (in agreement with refs. 18–20), and we demonstrate that this state suppresses Newtonian turbulence. In particular, we find that after the latter instability sets in, the flow directly approaches (with increasing *Re*) the MDR asymptote without any excursions to friction values indicative of Newtonian turbulence [note that a direct transition from laminar friction to MDR has also been seen in earlier studies (6), without relating it to an elastic instability, however]. Our observations imply that the MDR asymptote has its origin in the discovered instability and that it is dominated by elasticity. Although the instability mechanism is likely to be related to elastic turbulence, our studies are carried out in a different parameter regime where inertia cannot be neglected, and we therefore dub this state elasto-inertial turbulence (EIT). In addition, the existence of EIT and the direct approach to MDR are reproduced by direct numerical simulation

Author contributions: Y.D., C.W., and B.H. designed research; D.S., Y.D., M.H., C.S., and B.H. performed research; D.S., Y.D., M.H., C.S., and B.H. analyzed data; and Y.D., A.N.M., C.W., and B.H. wrote the paper.

The authors declare no conflict of interest.

*This Direct Submission article had a prearranged editor.

[1]To whom correspondence should be addressed. E-mail: bhof@ist.ac.at.

This article contains supporting information online at www.pnas.org/lookup/suppl/doi:10.1073/pnas.1219666110/-/DCSupplemental.

(DNS) of model viscoelastic fluid flow in a straight channel in the same range of Reynolds numbers as in the experiment. This suggests that the observed instability and friction scaling is characteristic for viscoelastic fluids in wall-bounded flows.

Results

At the lowest *Re* at which turbulence is sustainable in pipe flow, the turbulence appears (33) in the form of axially localized structures about 20 *D* in length, so-called "turbulent puffs." It has been shown that these structures decay back to laminar after sufficiently long times following a memoryless process (34, 35). Hence, for each *Re*, there is a distinct probability that a turbulent puff will survive beyond a certain time horizon. In the first set of measurements, this characteristic was used to quantify the influence of polymers on the transition to turbulence. Experiments were carried out in pipe flows for different polymer concentrations (50 ppm, 100 ppm, 125 ppm, 150 ppm, and 175 ppm). In all cases, the survival probability of puffs increases with the *Re* and, owing to the transient nature of the turbulent puffs, is only found to approach a probability of 1 asymptotically with the *Re* (Fig. 1*A*). Compared with pure water (Fig. 1*A*, blue curve), the curves are shifted to a larger *Re* as the concentration is increased, showing that the polymers delay transition and subdue turbulence. The *Re* required to reach a $P = 0.5$ survival probability is found to increase faster than linearly (Fig. 1*B*) with polymer concentration, providing a measure of the rate at which the turbulent state is postponed to a larger *Re* (i.e., transition delay).

Surprisingly, for polymer concentrations ≥200 ppm, turbulent puffs could not be detected; instead, a different type of disordered motion already sets in at a lower *Re*: Whereas in the Newtonian case, turbulent fluctuations can first be sustained for $Re \sim 2,000$ (Fig. 2*A*, open squares), in a 500-ppm solution, disordered motion was observed for a *Re* as low as 800 (Fig. 2*B*). Also, in Newtonian fluids, flows just above onset are intermittent [i.e., turbulent regions are interspersed by laminar regions (33); *SI Text*], whereas in the polymer solutions, fluctuations set in globally throughout the pipe (*SI Text*). The instability observed in polymer solutions hence leads to a qualitatively different type of disordered motion, EIT. A further distinction between the two types of turbulence is that in the Newtonian case, the onset is strongly hysteretic: Unperturbed flows remain laminar up to a large *Re* (to $Re = 6,500$ in our setup; black squares in Fig. 2 *A* and *C*), whereas perturbed flows display turbulence from around *Re* = 2,000. In contrast, in a 500-ppm solution, perturbed and unperturbed flows become turbulent at the same *Re* (Fig. 2*B*). Equally, friction factors follow the same scaling and directly approach the MDR asymptote (Fig. 2*D*) without any excursions toward the Newtonian turbulence (so-called "Blasius") friction scaling. This observation suggests that the MDR asymptote marks the characteristic drag of EIT rather than being the consequence of an asymptotic adjustment of ordinary turbulence.

Further inspection shows that the elasto-inertial instability also appears for lower polymer concentrations (<200 ppm). Here, the instability sets in at a larger *Re*, and hence in the regime where, in the presence of finite amplitude perturbations, flows already exhibit Newtonian-like (i.e., hysteretic, intermittent) turbulence. Starting from laminar flow without additional perturbations, we find that with an increasing *Re*, these more dilute solutions will unavoidably turn turbulent at a *Re* distinctly below the natural transition point ($Re = 6,500$) of this pipe, as shown for a 100-ppm solution in Fig. 2 *A* and *C* (solid triangles).

In contrast to the higher concentrations, the flow is intermittent here, consisting of localized turbulent regions (i.e., puffs) interspersed by nonlaminar, weakly fluctuating regions. As the *Re* is further increased, the spatial intermittency disappears and gives way to a uniformly fluctuating state and the friction values approach the MDR asymptote. The onset of instability is plotted in Fig. 3*A* as function of polymer concentration. Above the red curve in Fig. 3*A*, the flow has become unstable and the friction factor begins to approach the MDR asymptote. The green data points in Fig. 3*A* mark the appearance of turbulent puffs shown in Fig. 1*A* (i.e., the threshold where the puff $t_{1/2}$ exceeds $t = 760$ advective time units, which corresponds to the time for puffs to travel from the injection point to the observation point). For parameter settings between the red and green datasets in Fig. 3*A*, ordinary turbulence can be triggered by finite-amplitude perturbations, and the flow is hence hysteretic. On further increase of the *Re*, once the red curve in Fig. 3*A* is crossed, the flow will become unstable regardless of initial conditions.

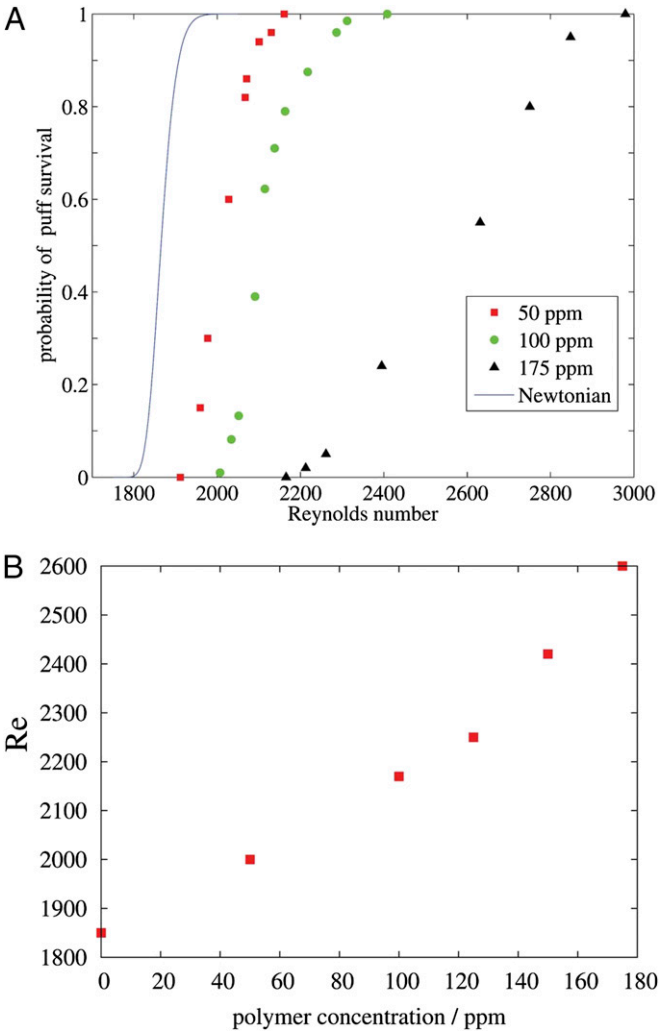

Fig. 1. Survival probability of turbulence. At the lowest *Re* at which turbulence can be observed in pipes, it has the form of localized structures that decay following a memoryless process (34, 35). The influence of polymers on this process is investigated for various concentrations. To create turbulence, the laminar flow was perturbed by an impulsive injection (of the same fluid) for 20 ms with sufficient amplitude to create a turbulent puff. The flow was then monitored at the exit of the pipe 760 *D* downstream by means of visual inspection using the same method as described by Hof et al. (34). Although for laminar flow, the fluid exits the pipe smoothly and follows a parabolic path, turbulent fluid (resulting from the different velocity profile) will exit the pipe at a different angle, causing a downward deflection and temporary distortion of the outflowing jet. By continuously monitoring the outflow, the survival probability of turbulent puffs was determined as a function of the *Re*. (*A*) Survival probabilities decrease for increasing polymer concentrations, and the survival probability found in the Newtonian case is only recovered at a larger *Re*. With increasing polymer concentration, the typical S-shape of the probability distributions becomes more pronounced. (*B*) *Re* with a 50% survival probability at the 760 *D* observation point as a function of polymer concentration.

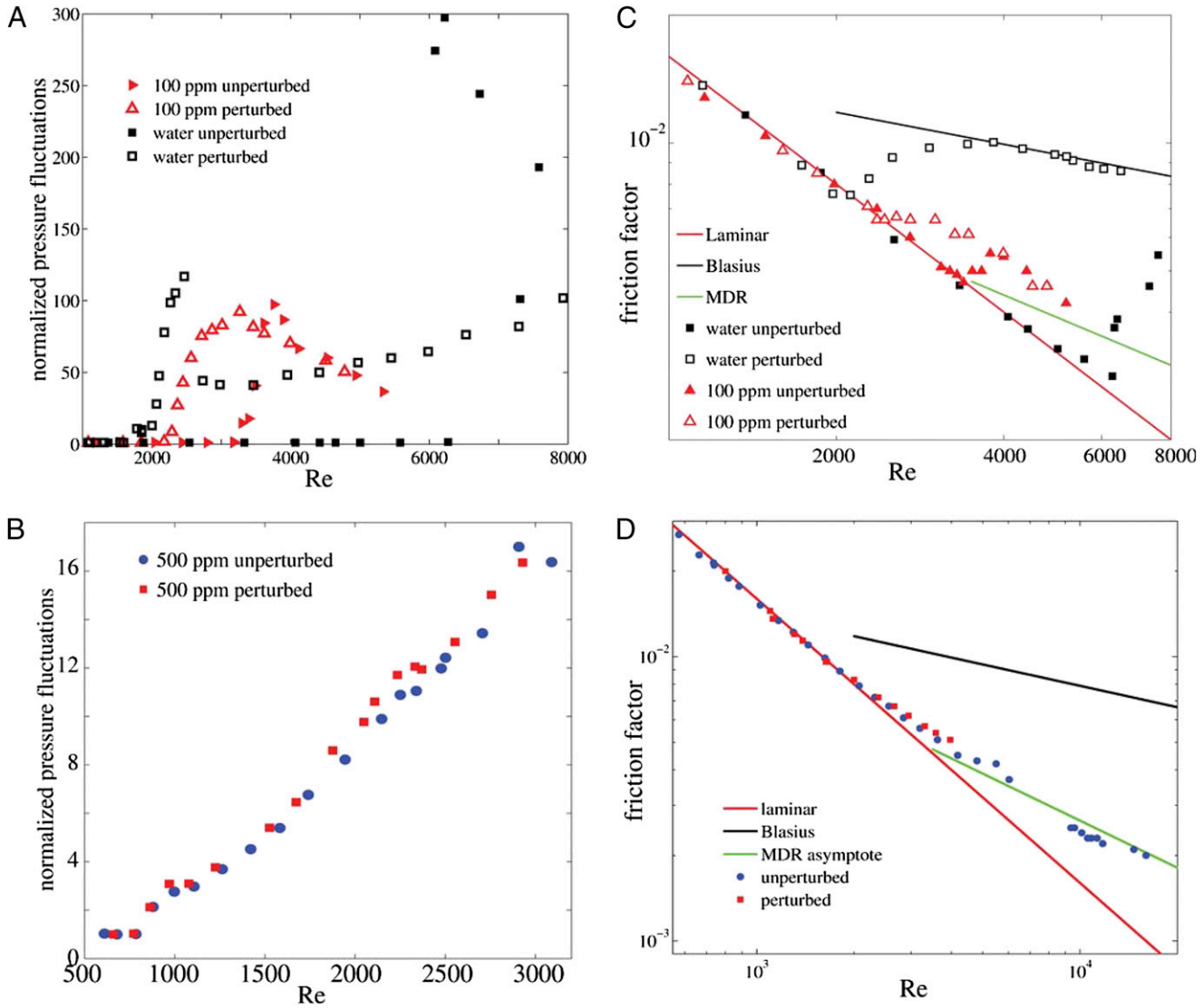

Fig. 2. Stability and friction scaling. (*A*) For the Newtonian case (black symbols), turbulence can first be triggered by perturbations for *Re* of about 2,000, where fluctuations increase rapidly. The quantity plotted is the fluctuation in pressure that was measured differentially between two pressure taps (1-mm holes in the pipe wall) separated by 3 *D* in the streamwise direction and located approximately 250 *D* from the pipe exit. (*B*) For a 100-ppm polymer solution (red data points), turbulence cannot be triggered below $Re = 2{,}200$ (transition delay). At $Re = 3{,}200$, however, instability occurs (even in the absence of perturbations), and this instability is caused solely by the presence of the polymers. At higher polymer concentrations (*B*; 500 ppm here), this instability occurs at a much lower *Re* and the hysteresis typical for Newtonian turbulence has disappeared (*A* and *C*). The flow already becomes unstable at $Re = 800$ (regardless of the presence of additional perturbations). From here (with an increasing *Re*), the flow directly approaches the MDR friction scaling (*D;* also for a concentration of 500 ppm).

Finally, experiments were carried out in pipes with diameters of $D = 2$ mm and $D = 10$ mm (blue and red data points in Fig. 3*B*). When plotting the stability thresholds observed in the three pipes in terms of shear rate vs. polymer concentration, all datasets collapse. The latter observation shows that the elasto-inertial instability scales with the shear rate and not with the *Re* (18). Hence, in tubes with a larger diameter, the instability will occur at a large *Re* and typically will be obscured by Newtonian turbulence. Inversely, on microscales, this instability will occur at a very low *Re*, opening new avenues for mixing in microchannels. Until recently, elastic turbulence and strong mixing had only been reported in curved channels (25, 36, 37), which are linearly unstable.

To gain further insights into the nature of the EIT, we conducted DNS of channel flow for a non-Newtonian fluid using a constitutive model extensively utilized in the simulation of polymer drag reduction. The numerical methods and rheological parameters are similar to those used in simulations of MDR (38, 39) (details are provided in *SI Text*). Great care was taken to resolve all flow scales relevant to the dynamics of such complex fluids requiring spatial and temporal resolutions significantly larger than for Newtonian turbulence. Each simulation is initially perturbed in such way that transition in Newtonian flow occurs at $Re = 6{,}000$, based on the bulk velocity U_b and channel height H.

In qualitative agreement with the experiments, we find that instability develops at a much lower *Re* in polymeric flows, which, again, directly leads to the MDR asymptote, as shown in Fig. 4*A* for $Re = 1{,}000$. Whereas the corresponding Newtonian flow is perfectly laminar, Fig. 4*B* shows pressure fluctuations on the lower wall of the channel, with a strong yet chaotic organization.

Closer inspection of the numerical data at the lowest simulated *Re*, $Re = 1{,}000$, reveals (Fig. 4*B*) an interesting topological structure of EIT. Even though the flow is dominated by the mean

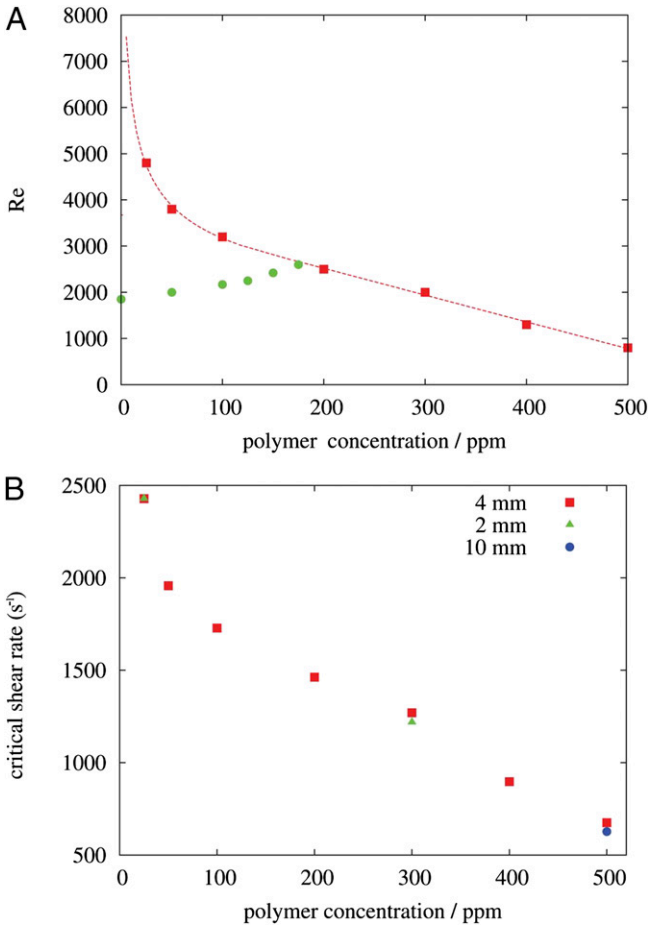

Fig. 3. Transition threshold to EIT is plotted for different concentrations (red squares). The red line is a guide for the eye. The green circles mark the transition delay to ordinary turbulence (Fig. 1*B*). Consequently, for concentrations below 200 ppm, the elasto-inertial instability sets in at a *Re* at which ordinary turbulence can already occur, whereas in the $D=4$-mm pipe, the elasto-inertial instability is found only above 200 ppm. (*B*) Red squares mark the critical shear rate for the onset of EIT in the 4-mm pipe (same as red squares in *A*). In addition, shear rates ($\dot{\gamma}=8U/D$) were determined for the flow in a $D=10$-mm pipe and a $D=2$-mm pipe. In these cases, the transition occurs at the same critical shear rate. Hence, unlike ordinary turbulence, the onset of EIT is not governed by the *Re* but, instead, by the shear rate.

shear, polymers are extended (large values of $\sqrt{tr(\mathbf{C})}/L$ see *Numerical Methods* and *SI Text*) in sheet-like regions of large streamwise (x) and spanwise (z) dimensions. The sheets are stretched at an upward angle from the streamwise direction, indicative of extensional flow topology. These sheets also produce larger polymer extension than the surrounding mean shear does; an increase of the effective flow viscosity, through extensional viscosity, is therefore confined to these very sheets. The response of the flow is observed in pressure fluctuations, shown in contours of wall pressure on the bottom wall of Fig. 4*B*. Fig. 4*C* shows isosurfaces of positive and negative Q, where $Q=-(1/2)\,\nabla\cdot(\nabla\cdot(\mathbf{u}\otimes\mathbf{u}))$ is the second invariant of the velocity gradient tensor and also a measure of the local flow topology (40). As shown, the flow is structured in alternating regions of rotational flows ($Q>0$) and extensional/compressional flows ($Q<0$). These regions are aligned in the spanwise direction and appear to have a large spanwise coherence scale of about one-third to one-half of the domain span. Note that this spanwise orientation is markedly different from Newtonian turbulence, where the dynamics are dominated by vortices oriented in the streamwise direction. At a larger *Re*, simulations show that after EIT sets in, flows contain streamwise–oriented as well as spanwise–oriented vortical structures. However, as the MDR asymptote is approached, with an increasing *Wi*, streamwise vortices are suppressed and the flow is dominated by spanwise structures, as in the case with a low *Re* shown in Fig. 4*B*.

Analogous to Newtonian turbulence also in the present simulations, perturbations of finite amplitude are required to trigger turbulence (albeit considerably smaller amplitude perturbations suffice). This suggests that as in Newtonian linearly stable shear flows (e.g., pipes), a self-sustaining mechanism is required to keep the turbulent motion alive. Whereas no hysteresis has been observed for the transition to EIT in the experiments (Fig. 2 *B* and *D*), this does not necessarily rule out that the instability may still be subcritical. If, as simulations suggest, very small (compared with the Newtonian case) finite-amplitude perturbations do indeed trigger turbulence, it may prove to be very difficult to reduce disturbance levels in experiments sufficiently to observe hysteresis. We propose that the underlying EIT is hence a self-sustaining cycle, wherein small-velocity perturbations cause the formation of sheets of extended polymers through convective transport. The flow response, through pressure, sustains velocity fluctuations, thereby closing the cycle.

Discussion and Conclusions

In summary, we have shown that small amounts of polymer added to a Newtonian solvent delay the transition point where Newtonian type turbulence can first be observed (i.e., resulting from a perturbation). At the same time, however, an elastic instability occurs at higher shear rates. At larger polymer concentrations, this elastic instability occurs at a *Re* sufficiently smaller than the transition in Newtonian pipe flow. In this regime of high elasticity, experimental measurements of friction factors for different polymer concentrations and different pipe diameters show that after this instability sets in, the friction factor follows the characteristic MDR friction law. This behavior is also confirmed by our numerical simulations, as can be seen from Figs. 2*D* and 4*A*. When we increase the *Re* further in our numerical simulations, we observe that the mean velocity profile approaches the Virk asymptote (Fig. 5*A*) and that the Reynolds stress becomes vanishingly small (Fig. 5*B*) at a large *Wi*. Both features are often quoted as the major characteristics of the MDR state (6, 16, 41). Our observation indicates that the MDR state is continuously linked to the EIT that we have discovered at relatively small *Re*.

It is noteworthy that the key elements of the mechanism of EIT (nonlinear advection of stress, stretching by flow and flow response via pressure) are common features to many viscoelastic fluids. Although EIT is possibly related to elastic turbulence, inertia cannot be neglected in our case, and there are no curved streamlines that would cause linear instability. Our observations infer that this type of fluid motion replaces ordinary turbulence and dominates the dynamics in elastic fluids at sufficiently large shear rates.

Materials and Methods

Experimental Methods. Experiments were carried out in a pipe made of ~1.2-m-long precision bore segments with an inner diameter of $D=(4\pm0.01)$ mm and a total length of about $L/D=900$. The flow was gravity driven, and the fluid temperature was controlled so that the flow rate could be held constant, typically to within $\pm0.2\%$ [details of a similar setup can be found in a study by de Lozar and Hof (42)]. The sample solutions were either pure water or different amounts of polyacrylamide with a molecular weight of 5×10^6 amu (PAAm; Sigma–Aldrich) in water. The shear viscosity increased with the polymer concentration, and almost no shear thinning was observed; however, a pronounced elastic behavior was found in the elongational flow of a capillary break-up elongational rheometer. The rheological characterization is given in *SI Text*. A carefully designed inlet of the pipe allowed us to keep flows of pure water laminar up to $Re\sim6,500$ (natural

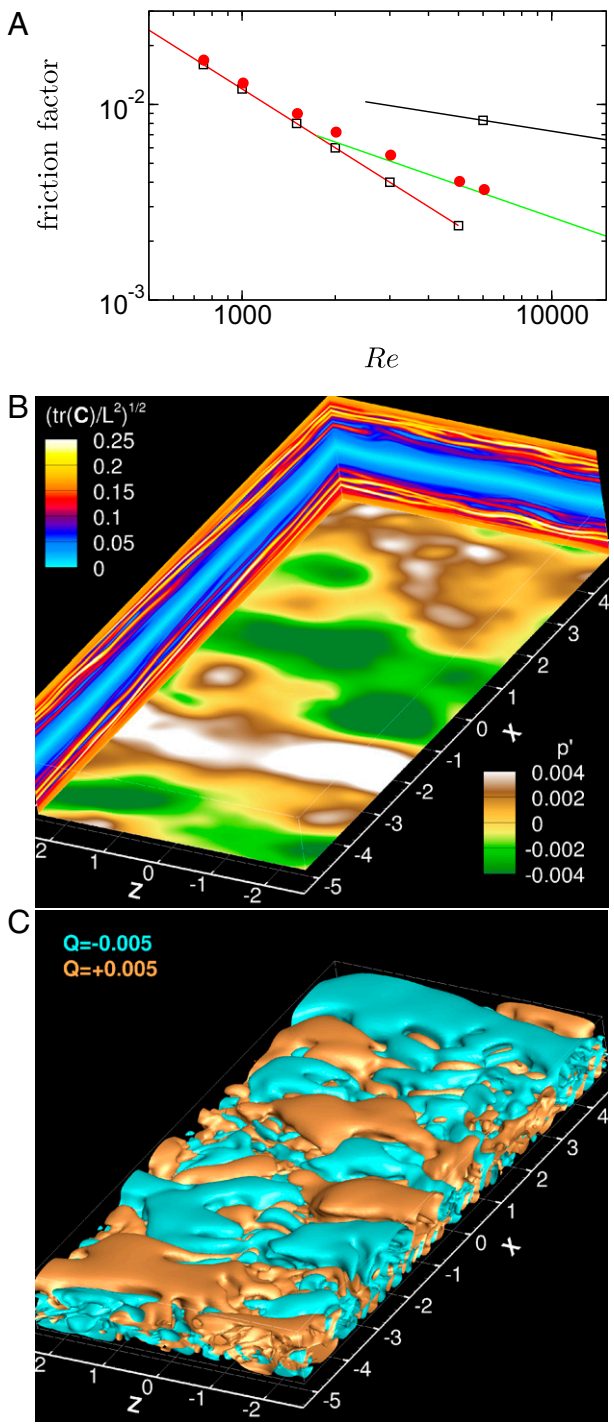

Fig. 4. Numerical simulation of EIT in a channel flow. (*A*) Red, green, and black lines highlight the laminar, turbulent, and MDR distributions of the friction factor, respectively, as a function of the *Re* based on the bulk velocity and the height of the channel. The simulations are performed in a channel flow of large transversal dimensions with periodic boundary conditions in horizontal dimensions. At time $t = 0$, a perturbation is introduced in the form of space and time oscillations of blowing and suction at the walls for a fixed, short duration. The intensity of the perturbations is tailored so that a transition is triggered at $Re = 6{,}000$ for the simulated water flow. Using the same perturbation, the simulated polymeric channel flow already shows a departure from purely laminar flow at around $Re = 750$ (red circles). (*B*) Contours of pressure fluctuations on the bottom wall and polymer stretch in vertical planes ($Re = 750$). (*C*) Isosurfaces of regions of slightly rotational (orange) or extensional (cyan) nature ($Re = 750$), as identified by the second invariant of the velocity tensor *Q* (details are provided in *SI Text*).

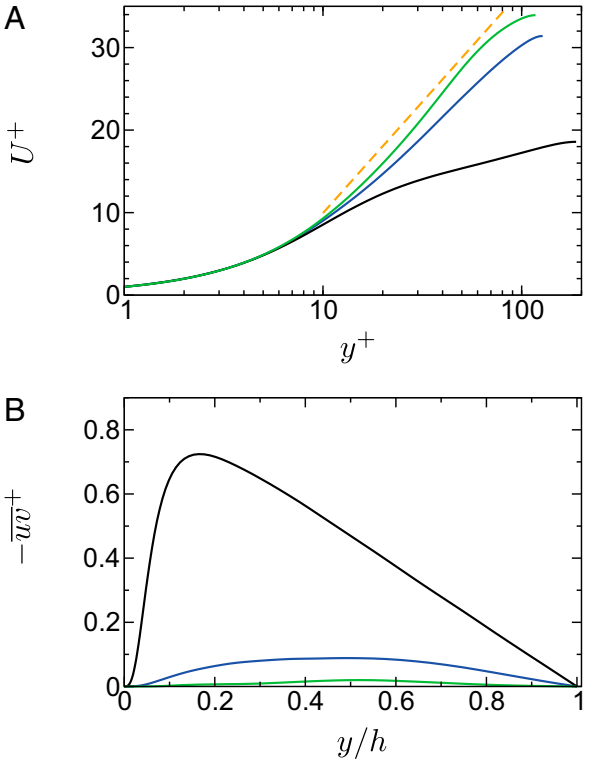

Fig. 5. Profiles of turbulence statistics at the highest simulated *Re* with the addition of a higher *Wi* simulation. For FENE-P fluids (see *SI Text*), $Wi \gg 1$ leads to a universal form of the polymer tensor closely related to the MDR asymptotic state. Mean velocity profiles in the typical log-linear representation are shown, where the mean velocity U^+ and the distance from the wall y^+ are normalized by skin-friction velocity u_τ and kinematic viscosity (*A*) vs. profiles of Reynolds shear stress, $-\overline{uv}^+ = -\overline{uv}/u_\tau^2$, as a function of the distance from the wall normalized by the channel half-height *h* (*B*). Statistics are shown for $Re = 6{,}000$; solid blue line, $Wi = 100$; solid green line, $Wi = 700$; solid black line, Newtonian turbulent flow. (*A*) Virk log-law (6) is denoted by the dashed orange line. The Virk mean velocity profile is a best fit of high *Re* data. The assumption of the existence log-law at a low *Re* was recently shown (39) to fail at a low to moderate *Re* (at least up to $Re = 10{,}000$). The agreement of $Wi = 700$ is consistent with previous MDR simulations and experiments. (*B*) Experiments of Warholic et al. (41) at MDR observe negligible Reynolds shear stress.

transition point for this pipe). Here, the *Re* is defined as $Re = UD/\nu$, where *U* is the mean flow speed and ν is the kinematic viscosity. Although laminar (Newtonian) pipe flow is stable for all *Re*, turbulence of appreciable lifetime can be triggered by perturbations of finite amplitude once the *Re* approaches 2,000 (34, 43). In the present setup, turbulence was triggered by injecting fluid through a small hole in the pipe wall situated 140 *D* from the inlet; alternatively, for continuous triggering of turbulence, an obstacle (~2-cm-long ~1-mm-thick twisted wire) could be placed downstream of the inlet.

Numerical Methods. The flow is governed by the incompressible Navier–Stokes equations with the addition of a viscoelastic stress using the Finitely Extensible Nonlinear Elastic-Peterlin (FENE-P) model:

$$\partial_t \mathbf{u} + \mathbf{u}\cdot\nabla\mathbf{u} = -\nabla p + \frac{\beta}{Re}\nabla^2\mathbf{u} + \frac{1-\beta}{Re}\nabla\cdot\mathbf{T}, \quad [1]$$

$$\nabla\cdot\mathbf{u} = 0, \quad [2]$$

in a rectangular domain with periodic boundary conditions in the streamwise and spanwise directions, and no slip at the walls, where $\mathbf{u}$ is the velocity vector and p is the pressure. The flow is driven by a bulk force to maintain a constant mass flow rate. The velocity and length scales used to form the *Re* and to normalize the flow variables are the bulk velocity and the height of

the channel, respectively. The polymer stress tensor **T** in Eq. **2** is derived from the following transport equation:

$$\partial_t \mathbf{C} + \mathbf{u}\cdot\nabla\mathbf{C} = \mathbf{C}\cdot\nabla\mathbf{u} + \nabla\mathbf{u}^T\cdot\mathbf{C} - \mathbf{T}, \quad [3]$$

with

$$\mathbf{T} = \frac{1}{Wi}(f(\mathbf{C})\mathbf{C} - \mathbf{I}), \quad [4]$$

$$f(\mathbf{C}) = \frac{1}{1 - tr\mathbf{C}/L^2}, \quad [5]$$

where **C** is the conformation tensor and f is the Peterlin function based on L, the upper limit of polymer extension. The polymer solution is characterized by the Wi, which is the ratio of polymer relaxation time to flow scale: here, it is the inverse of the wall shear. In Eq. **2**, the coefficient β is the ratio of the solvent viscosity to the zero-shear viscosity of the polymer solution. The numerical method used to solve Eqs. **2** and **3** is described by Dubief et al. (38) and is briefly introduced here. The flow is discretized on a staggered grid. Velocity derivatives are computed with second-order, energy-conserving, finite-difference schemes. The divergence of the polymer stress tensor in Eq. **3** uses a fourth-order compact central scheme. To accommodate the sharp gradients arising from Eq. **3**, the advection term is discretized with a third-order compact upwind scheme, supplemented by local artificial dissipation. The upper boundedness of the polymer conformation tensor is guaranteed by an algorithm described by Dubief et al. (38). Time advancement uses the typical fractional step method utilized in most DNSs of turbulence.

The rheological parameters adopted here are consistent with those used in previous simulations of polymer drag reduction (11, 12, 44–46). We use a maximum polymer extension of $L = 200$, $\beta = 0.9$, and $Wi^* = 8$. Here, Wi^* is the polymer relaxation time divided by the integral flow time scale (ratio of the channel half-height to bulk velocity). The increase in Re is achieved by decreasing the velocity, while keeping the channel height and bulk velocity constant. The Wi of interest is based on the wall shear of the corresponding Newtonian flow. Consequently, the Wi is equal to 24 in the laminar region and is 100 for $Re = 6{,}000$. The highest Wi discussed in Fig. 5 corresponds to $Wi^* = 60$.

The computational domain dimensions and resolution are 10 $H \times H \times 5$ H and $256 \times 161 \times 256$, respectively. For polymer flows, the streamwise Δx^+ and spanwise Δz^+ resolutions, normalized by their respective viscous scales, range from $\Delta x^+ \in [1.5, 5]$ and $\Delta z^+ \in [0.75, 2.5]$ across the range of $Re \in [1{,}000, 6{,}000]$. In the same range of Re, the minimum and maximum cell sizes in the wall normal direction are within [0.01, 0.05] and [1.5, 5]. Doubling the dimensions and resolution in transversal directions or increasing the resolution in the wall normal direction did not yield any appreciable change in statistics.

ACKNOWLEDGMENTS. D.S. and C.S. were partly funded by Deutsche Forschungsgemeinschaft Project WA1336-5-1. A.N.M. was funded by the Engineering and Physical Sciences Research Council (Grant EP/I004262/1).

1. Toms BA (1948) Some observations on the flow of linear polymer solutions through straight tubes at large Reynolds numbers. *Proceedings of the First International Congress on Rheology* 2:135–141.
2. Sreenivasan KR, White CM (2000) The onset of drag reduction by dilute polymer additives, and the maximum drag reduction asymptote. *J Fluid Mech* 409:149–164.
3. White CM, Mungal MG (2008) Mechanics and prediction of turbulent drag reduction with polymer additives. *Annu Rev Fluid Mech* 40:235–256.
4. Sellin RHJ, Ollis M (1980) Polymer drag reduction in large pipes and sewers: Results of recent field trials. *J Rheol (N Y N Y)* 24(5):667–684.
5. Khalil MF, Kassab SZ, Elmiligui AA, Naoum FA (2002) Applications of drag-reducing polymers in sprinkler irrigation systems: Sprinkler head performance. *Journal of Irrigation and Drainage Engineering (ASCE)* 128(3):147–152.
6. Virk PS, Mickley HS, Smith KA (1970) The ultimate asymptote and mean flow structure in Toms phenomenon. *Journal of Applied Mechanics - ASME* 37(2):488–493.
7. Giles WB, Pettit WT (1967) Stability of dilute viscoelastic flows. *Nature* 216:470–472.
8. Dimitropoulos CD, Sureshkumar R, Beris AN, Handler RA (2001) Budgets of Reynolds stress, kinetic energy and streamwise enstrophy in viscoelastic turbulent channel flow. *Phys Fluids* 13(4):1016–1027.
9. Min T, Yoo JY, Choi H, Joseph DD (2003) Drag reduction by polymer additives in a turbulent channel flow. *J Fluid Mech* 486:213–238.
10. Stone PA, Roy A, Larson RG, Waleffe F, Graham MD (2004) Polymer drag reduction in exact coherent structures of plane shear flow. *Phys Fluids* 16(10):3470–3482.
11. Dubief Y, et al. (2004) On the coherent drag-reducing and turbulence-enhancing behaviour of polymers in wall flows. *J Fluid Mech* 514:271–280.
12. Li CF, Sureshkumar R, Khomami B (2006) Influence of rheological parameters on polymer induced turbulent drag reduction. *J Nonnewton Fluid Mech* 140(1-3):23–40.
13. Roy A, Morozov A, van Saarloos W, Larson RG (2006) Mechanism of polymer drag reduction using a low-dimensional model. *Phys Rev Lett* 97(23):234501.
14. Kim K, Adrian RJ, Balachandar S, Sureshkumar R (2008) Dynamics of hairpin vortices and polymer-induced turbulent drag reduction. *Phys Rev Lett* 100(13):134504.
15. Xi L, Graham MD (2010) Turbulent drag reduction and multistage transitions in viscoelastic minimal flow units. *J Fluid Mech* 647:421–452.
16. Xi L, Graham MD (2012) Dynamics on the laminar-turbulent boundary and the origin of the maximum drag reduction asymptote. *Phys Rev Lett* 108(2):028301.
17. Draad AA, Kuiken GDC, Nieuwstadt FTM (1998) Laminar-turbulent transition in pipe flow for Newtonian and non-Newtonian fluids. *J Fluid Mech* 377:267–312.
18. Ram A, Tamir A (1964) Structural turbulence in polymer solutions. *J Appl Polym Sci* 8(6):2751–2762.
19. Little RC, Wiegand M (1970) Drag reduction and structural turbulence in flowing polyox solutions. *J Appl Polym Sci* 14(2):409–419.
20. Ostwald W, Auerbach P (1926) The viscosity of colloidal solutions in the area of structure, laminar and turbulence. *Kolloid Zeitschrift* 38:261.
21. Paterson RW, Albernathy FH (1972) Transition to turbulence in pipe flow for water and dilute solution of polyethylene oxide. *J Fluid Mech* 51:177–185.
22. Larson RG, Shaqfeh ESG, Muller SJ (1990) A purely elastic instability in Taylor Couette flow. *J Fluid Mech* 218:573–600.
23. Shaqfeh ESG (1996) Purely elastic instabilities in viscometric flows. *Annu Rev Fluid Mech* 28:129–185.
24. Groisman A, Steinberg V (2000) Elastic turbulence in a polymer solution flow. *Nature* 405(6782):53–55.
25. Groisman A, Steinberg V (2001) Efficient mixing at low Reynolds numbers using polymer additives. *Nature* 410(6831):905–908.
26. Ho TC, Denn MM (1977) Stability of plane Poiseuille flow of a highly elastic liquid. *J Nonnewton Fluid Mech* 3(2):179–195.
27. Morozov AN, van Saarloos W (2007) An introductory essay on subcritical instabilities and the transition to turbulence in visco-elastic parallel shear flows. *Phys Rep* 447:112–143.
28. Bonn D, Ingremeau F, Amarouchene Y, Kellay H (2011) Large velocity fluctuations in small-Reynolds-number pipe flow of polymer solutions. *Phys Rev E Stat Nonlin Soft Matter Phys* 84(4 Pt 2):045301.
29. Pan L, Morozov A, Wagner C, Arratia PE (2013) Nonlinear elastic instability in channel flows at low Reynolds numbers. Phys. *Rev Lett* 110:174502.
30. Fouxon A, Lebedev V (2003) Spectra of turbulence in dilute polymer solutions. *Phys Fluids* 15(7):2060–2072.
31. Boffetta G, Celani A, Mazzino A (2005) Drag reduction in the turbulent Kolmogorov flow. *Phys Rev E Stat Nonlin Soft Matter Phys* 71(3 Pt 2B):036307.
32. Watanabe T, Gotoh T (2010) Coil-stretch transition in an ensemble of polymers in isotropic turbulence. *Phys Rev E Stat Nonlin Soft Matter Phys* 81(6 Pt 2):066301.
33. Hof B, de Lozar A, Avila M, Tu X, Schneider TM (2010) Eliminating turbulence in spatially intermittent flows. *Science* 327(5972):1491–1494.
34. Hof B, Westerweel J, Schneider TM, Eckhardt B (2006) Finite lifetime of turbulence in shear flows. *Nature* 443(7107):59–62.
35. Hof B, de Lozar A, Kuik DJ, Westerweel J (2008) Repeller or attractor? Selecting the dynamical model for the onset of Turbulence in Pipe flow. *Phys Rev Lett* 101(21):214501.
36. Burghelea T, Segre E, Steinberg V (2004) Mixing by polymers: Experimental test of decay regime of mixing. *Phys Rev Lett* 92(16):164501.
37. Jun Y, Steinberg V (2010) Mixing of passive tracers in the decay Batchelor regime of a channel flow. *Phys Fluids* 22(12):123101.
38. Dubief Y, et al. (2005) New Answers on the Interaction Between Polymers and Vortices in Turbulent Flows. *Flow Turbulence and Combustion* 74(4):311–329.
39. White CM, Dubief Y, Klewicki J (2012) Re-examining the logarithmic dependence of the mean velocity distribution in polymer drag reduced wall-bounded flow. *Phys Fluids* 24(2):021701.
40. Chong MS, Perry AE, Cantwell BJ (1990) A general classification of three-dimensional flow fields. *Physics of Fluids A* 2(5):765–777.
41. Warholic MD, Massah T, Hanratty TJ (1999) Influence of drag-reducing polymers on turbulence: Effects of Reynolds number, concentration and mixing. *Exp Fluids* 26(5):461–472.
42. de Lozar A, Hof B (2009) An experimental study of the decay of turbulent puffs in pipe flow. *Philos Trans A Math Phys Eng Sci* 367(1888):589–599.
43. Avila K, et al. (2011) The onset of turbulence in pipe flow. *Science* 333(6039):192–196.
44. Housiadas KD, Beris AN (2006) Extensional behavior influence on viscoelastic turbulent channel flow. *J Nonnewton Fluid Mech* 140(1-3):41–56.
45. Tamano S, Itoh M, Hotta S, Yokota K, Morinishi Y (2009) Effect of rheological properties on drag reduction in turbulent boundary layer flow. *Phys Fluids* 21(5):055101.
46. Dallas V, Vassilicos JC, Hewitt GF (2010) Strong polymer-turbulence interactions in viscoelastic turbulent channel flow. *Phys Rev E Stat Nonlin Soft Matter Phys* 82(6 Pt 2):066303.